On the Heterogeneity of the Earthquake Rupture

Luca Malagnini[1], Douglas S. Dreger[2], Robert M. Nadeau[2], Irene Munafò[1], and Massimo Cocco[1]

1. Istituto Nazionale di Geofisica e Vulcanologia, Via di Vigna Murata 605, Rome, Italy.

2. Berkeley Seismological Laboratory, University of California Berkeley.

Corresponding author: Luca Malagnini (luca.malagnini@ingv.it)

SUMMARY

The scaling of earthquake parameters with seismic moment and its interpretation in terms of self-similarity is still debated in the literature. We address this question by examining a worldwide compilation of corner frequency-based and elastic rebound theory (ERT)-based fault slip, area and stress drop values for earthquakes ranging in magnitude from -0.7 to 7.8. We find that corner frequency estimates of slip (and stress drop) scale differently than those inferred from the ERT approach, where the latter deviates from the generally accepted constant stress drop behavior of so-called self-similar scaling models. We also find that average slips from finite-source models are consistent with corner frequency scaling, whereas peak slip values are more consistent with the ERT scaling. The different scaling of corner frequency- and ERT-based estimates of slip and stress drop with earthquake size is interpreted in terms of heterogeneity of the rupture process. ERT-based estimates of stress drop decrease with seismic moment suggesting a self-affine behavior. Despite the inferred heterogeneity at all scales, we do not observe a clear effect on the Brune stress drop scaling with earthquake size.

Keywords: Earthquake dynamics; Earthquake source observations; Dynamics and mechanics of faulting. **Issue Section:** Seismology

INTRODUCTION

The great body of seismological investigations into earthquake rupture parameters suggests that stress drop is constant over the full range of earthquake magnitude, and that the source parameters of rupture area and slip scale in a self-similar manner (Aki, 1972; Hanks, 1977; Ide & Beroza, 2001; Kanamori and Anderson, 1975), although there is some evidence for non-self-similar scaling (e.g. Malagnini et al., 2010; Mayeda and Malagnini, 2009; Mayeda et al., 2007; Nadeau and Johnson, 1998). Although demonstrating the self-similar behavior of earthquake ruptures from the scaling of stress drop and earthquake parameters with seismic moment is still an open question and a debated issue (Cocco et al., 2016), in this paper we will refer to self-similar behavior to describe the constant scaling of stress drop with earthquake size. The scaling of source parameters with earthquake size is of paramount relevance for understanding the mechanics of earthquakes and faulting and seismic hazard assessment. This typically involves the estimation of single-number descriptors such as rupture area, slip and stress drop, which tacitly implies spatial averaging of the parameter over the assumed fault plane (Noda et al., 2013; Cocco et al., 2016). Earthquake source parameters are commonly inferred from recorded waveforms, either assuming a point-source representation (Brune, 1970; Brune, 1971; Madariaga, 1976; Sato & Hirasawa, 1973), or from the inversion of geophysical data to define finite-source models (Bletery et al., 2014; Dreger et al., 2007a; Kim et al., 2016). The former approach provides a single estimate of the source parameters for each investigated earthquake, whereas the latter yields information on the spatially and

temporally varying slip, slip velocity, and rupture speed, from which peak and mean values of slip can be determined.

In this study we compile source parameter estimates of earthquakes from sequences from diverse tectonic settings around the world (Figure 1) using three different and complementary methods, and we discuss the scaling of slip and stress drop with earthquake size. We interpret the differences in the inferred scaling laws in terms of the heterogeneity of earthquake rupture. In the following we provide background on the three independent methods: corner frequency based, elastic rebound based, and finite-source methods.

Corner Frequency Approach

The most widely used class of approaches for point-source determination of earthquake parameters relies on the spectral analysis of seismograms to measure corner frequencies (f_c) and seismic moments (M_0) (e.g. Malagnini et al., 2014a; Malagnini et al., 2014b), and we refer to these approaches as Brune-based (see Appendices subsection for details). Assuming the inverse proportionality scaling between the event's corner frequency (f_c) and the linear source dimension (i.e., the equivalent source radius) (eqn 1), the coseismic slip and the static stress drop of an earthquake obtained using a Brune-based approach are model-dependent.

Although different theoretical relationships are available in the literature (Brune, 1970; Brune, 1971; Madariaga, 1976; Sato & Hirasawa, 1973, Kaneko and Shearer, 2014), they differ only by the scaling constants between f_c and the source radius, contributing to epistemic uncertainties in stress drop of up to a factor of 5.58 (Zollo et al., 2014). The rupture dimension estimated from the earthquake's corner frequency is then used to determine source parameters such as rupture area, slip, and stress drop. The following equations describe the relationships between measured corner frequency and estimated source parameters:

$$L = c\frac{V_R}{f_c} \quad (1)$$

$$\Delta\sigma \approx \mu\frac{\bar{u}}{L} \propto \frac{M_0}{L^3} \quad (2)$$

$$L \propto {M_0}^{1/3} \quad (3)$$

$$\bar{u} \propto {M_0}^{1/3} \quad (4)$$

$$f_c \propto \frac{V_R}{{M_0}^{1/3}} \quad (5)$$

The coefficient c in equation (1) is a scale parameter specific to the three models that are commonly applied (Brune, 1970; Sato and Hirasawa, 1973; Madariaga, 1976). V_R is the rupture velocity, f_c is the measured corner frequency, and L is the fault dimension (the radius in the aforementioned models). The stress drop, rigidity, average slip, and scalar seismic moment are denoted as $\Delta\sigma$, μ, $\bar{u}$, and M_0. Rupture area and average slip scale as $1/f_c^2$, and stress drop scales as f_c^3. Thus relatively small errors in corner frequency translate to large uncertainties in derived parameters that is compounded by bias that can be introduced through incomplete coverage of the focal sphere for these simple models. Despite these large internal uncertainties, and the compounding epistemic uncertainty, these approaches remain the most commonly used method to estimate source dimension, coseismic slip and stress drop.

The work by Malagnini, Mayeda, and co-workers (a summary of which is given for a number of different seismic sequences in Malagnini et al., 2014b) shows that estimates of stress drop from earthquakes within individual mainshock-aftershock seismic sequences always steadily increase with increasing moment magnitude (interpreted as a breakdown from self-similar behavior). Yet, the compilation of all stress drop estimates from all the different seismic sequences

appears to be independent of seismic moment (a result interpreted as self-similar behavior, see Figure 2 and Cocco et al., 2016).

We point out that the findings from individual seismic sequences by Malagnini et al. (2014b) are in good agreement with the results by Blanke et al., (2019), who describe a steady increase of stress drop of lab-created acoustic emissions with increasing magnitude, although the compounded data set compiled of all individual sequences shows a fairly constant stress drop with increasing magnitude (Figure 3). It is worth noticing that, whereas a set of the stress drops from an individual seismic sequence is affected by a moderate scatter, large compilations of stress drop estimates from multiple seismic sequences occurring in different regions of the world suffer from huge scatter, up to a factor of 3 orders of magnitude (Cocco et al., 2016). What just described should make us very cautious when we try to interpret earthquake source scaling in terms of self-similar vs. non-self-similar physical processes.

Elastic Rebound Theory (ERT) Approach

The ERT approach was first proposed by Nadeau and Johnson (1998), who showed that the repeating nature of micro earthquakes on the Parkfield segment of the San Andreas fault can be used to determine the individual event slip assuming the known geodetic loading rate and an independent estimate of the scalar moment (typically from a spectral measurement) to determine the rupture area. They observed that the repeat times depended strongly on the magnitude of the earthquake. This method assumes that slip that occurs in the rapid, radiating seismic process keeps pace with the overall loading rate, and a model consisting of high strength asperities (of varying dimension) are locked and steadily accumulating stress through the strain of adjacent material creep. This method estimates a rupture dimension that is independent of a spectral corner frequency, and it also results in a significant so-called non-self-similar scaling of the slip and stress drop which has

been strongly debated (Ide and Beroza, 2001; Mayeda et al., 2007). The non-self-similar scaling *a la* Nadeau and Johnson (1998) has the opposite behavior as described above for sequences of events, and the stress drop appears to decrease with increasing scalar seismic moment, where the slip is found to scale as $M_0^{-1/6}$ and the stress drop as $M_0^{-1/4}$, apparently deviating from so-called self-similarity (Nadeau and Johnson, 1998).

Finite-Source Modeling Approach

The third method that can recover information about the slip and stress drops of earthquakes involves finite-source modeling (e.g. Olsen and Apsel, 1982; Hartzell and Heaton, 1983). In such modeling the waveforms are inverted for the spatial and temporal distribution of fault slip. The models are parameterized with slip velocity and rupture velocity kinematic parameters, and do assume a fault geometry from aftershock distributions, a focal mechanism, and possibly field observation of faulting. Typically, the fault orientation is examined through forward modeling to find a preferred fault geometry. These models can allow for complications in terms of multiple fault planes and non-planar rupture, as well as spatio-temporal heterogeneous slip. They account for the rupture kinematics, and also for the directivity that affects pulse widths and corner frequencies. However, finite-source inversions are non-unique owing to the underdetermined nature of the inversion as well as differences in kinematic parameterizations, and differences in reported solutions for a given earthquake can be seen in the literature (e.g. Bresnev, 2003; Mai et al. 2016; Wang et al., 2020). Further, such models are commonly regularized by slip positivity and smoothing constraints. Despite this, the finite-source models are useful because they directly estimate the slip and the rupture dimension, while taking into account the effects of propagating rupture and associated directivity. All published models show heterogeneity in slip where there are high-slip concentrations (interpreted as asperities) and regions of lower slip. High slip patches

(asperities) can be located far away from the rupture onset and the slip gradient controls the stress drop distribution on the fault plane. For this reason, the slip models can be used to estimate the stress changes on the fault (Ripperger & Mai, 2004) from which the average and peak values can be determined.

The epistemic uncertainties within Brune-based and FSM-based, as well as between the two approaches, partially explains the observed large dispersion in the scaling of earthquake stress drop with earthquake size that is reported in the literature. Despite the epistemic uncertainty, as well as the errors in the individual estimates of corner frequency and stress drop, the average stress drop of large heterogeneous data sets, sampling multiple regions of the world and multiple seismic sequences, is generally found to be essentially constant (varying between 0.1 to 10 MPa) over a range of more than 10^{20} in scalar seismic moment (Aki, 1972; Hanks, 1977; Ide & Beroza, 2001; Kanamori, 1975; Cocco et al., 2016). This is interpreted in terms of self-similar scaling of rupture area, source dimension, and average slip, with scalar seismic moment.

In this paper we analyzed a collection of M_0-slip data from earthquakes located worldwide (Fig. 1), together with those obtained in this study from 1811 repeating earthquakes that occurred along the creeping section of the SAF at Parkfield (Fig. S1 in the Supporting Information). We use both Brune-based and ERT-based approaches to estimate slip and stress drop, as well as results from published finite-source modeling.

In what follows we will show results and discuss interpretations about global observations, and the main contribution of this work concerning the transitional segment of the San Andreas fault at Parkfield (CA). The reason for such an apparent imbalance in analyzing the results from these different observations is that we want to extend the range of earthquake magnitudes for the ERT-based source parameters towards the small-magnitude end of the spectrum. In order to do so, we

needed a seismic network with exceptional characteristics (long recording history, dense, and equipped with low-noise borehole stations), which were all present in the High Resolution Seismic Network (HRSN) at Parkfield.

RESULTS

The 1811 repeating earthquakes are organized in 163 tight clusters ($0.4 < \mathbf{M} < 1.6$, **M** being moment magnitude, see Malagnini & Dreger, 2016). The Parkfield data set comprises a total of 38,124 selected waveforms recorded at 12 borehole stations of the High Resolution Seismic Network (HRSN), extracted from the repository of the Northern California Earthquake Data Center (NCEDC).

We calculate the spectral ratios between all the excitation spectra provided by Malagnini & Dreger (2016), and the spectrum of a single reference event (evt # 587 in Malagnini & Dreger, 2016; Cluster C32 of Table S1 in the Supporting Information; temporal ID: 2004343071645). We use a stable optimization technique for the calculation of the events' corner frequencies that utilizes virtually co-located seismic events to account for attenuation effects on their spectra (Malagnini et al., 2014a). However, due to the inherent difficulties of the analysis of the recorded micro-earthquakes (the corner frequencies of most events of the Parkfield data set are outside the available bandwidth), we succeed in calculating stable corner frequencies for only 21 repeating events (see Table S1 of the Supporting Information). We used the Brune spectral model to obtain Brune-based source-radii from their corner frequencies and with estimates of their seismic moments calculated slip and stress drops. The slip values inferred from spectral analysis are indicated by red symbols in Figure 2.

The Brune-based estimates obtained in this study for the Parkfield data set, together with those computed in other regions of the world with the same method (Malagnini et al., 2014a;

Malagnini et al., 2014b), relate the slip inferred from corner frequency measurements of earthquakes spanning a 10^{13} range in scalar seismic moment. To first order, as shown in numerous other studies (Aki, 1972; Hanks, 1977; Ide & Beroza, 2001; Kanamori and Anderson, 1975), such values are consistent with the $M_0^{1/3}$ self-similar scaling law. Thin dashed lines in Figure 2 display the so-called self-similar scaling law (2), which is expected for a constant Brune stress drop model. Red and black dashed lines identify, respectively, the slip scaling inferred for the Brune (1970, 1971) and the Madariaga (1976) relations between corner frequency and source radius. For the Parkfield repeaters, different symbols indicate the Brune-based slip estimates for earthquakes that occurred before and after the 2004 main shock, however no systematic differences can be detected between the two subsets of Parkfield data.

We also computed estimates of slip and stress drop for the Parkfield repeating earthquakes under the hypothesis that the entire long-term slip rate of the SAF (0.023 m/year from Nadeau & Johnson, 1998) is accommodated seismically by the clusters of repeating micro-earthquakes occurring along its creeping section, and using the seismic moments calculated by Malagnini & Dreger (2016). In this ERT-based (Nadeau & Johnson, 1998) approach we imposed the requirement that the cumulative slip integrated over all the repeaters of each cluster in an undisturbed time window (e.g., with no other perturbation such as loading from nearby earthquakes, or post-seismic processes) matches the long-term tectonic load of the SAF at Parkfield (0.023 m/year). For each cluster, we performed a grid-search over its stress drop in the undisturbed time window, given the hypotheses that the stress drop remains constant through time, and is common to all the events belonging to the specific cluster. We chose the stress drop that allows the specific set of repeating earthquakes to slip a cumulative amount obtained by multiplying the duration of the available time window by the long-term slip rate of 0.023 m/year (see Table S2). This cumulative slip is then

distributed to the individual events by how many times they repeat in the available time window. Cyan symbols in Figure 2 represent ERT-based slip estimates.

The ERT-based theoretical slip values follow the scaling proposed by Nadeau & Johnson (1998) which predicts:

$$\bar{u} \propto {M_0}^{1/6} \quad (6)$$

In Figure 2 we also plot the average and the peak slip values retrieved from finite source models (Dreger et al., 2007a; Kim et al., 2016; Taira et al., 2015) (yellow squares and hexagons, respectively) for several earthquakes (see the legend in the figure) as well as the slip values computed in this study through the ERT-based approach (cyan symbols).

Figure 2 corroborates three important results. First, peak slip values obtained from finite source models are very similar to the ERT-based slip values, and trend in the same manner as the scaling law described in (6). Peak slip in finite-source models is sensitive to the degree of discretization of the model, and to the smoothing constraints in the inversion. Models are developed by finding the smoothest distributions of slip that retain a high level of fit with the data, in addition the smoothing is chosen such that the dimensions of features in the slip models are consistent with the minimum wavelength of data used in the inversion. However, the results presented are from several independent studies, distinct numerical approaches and different analysts and therefore the consistency of peak slip with the ERT-based slip values is unexpected, and can be considered significant. Second, the average slip values obtained from finite source models are very similar to the Brune-based point-source estimates and follow the same scaling predicted by (4), corroborating the lack of stress drop scaling with seismic moment (Cocco et al., 2016). There might be differences between the finite-source average slip values and the Brune-based estimates, but these

discrepancies lie within the dispersion of inferred values. Cocco et al. (2016) have discussed the large (three decades) dispersion in stress drop estimates. Third, on a compilation of data from multiple seismic sequences from different tectonic regions of the world, the scaling of the Brune-based stress drop is constant throughout 13 orders of magnitude in seismic moment (see also Fig. 3), corroborating previous independent results (Cocco et al., 2016).

Our ERT-based slip estimates of the Parkfield repeaters (cyan triangles in Fig. 2) nicely overlap with data obtained by Nadeau & Johnson (1998) using the same assumptions (cyan diamonds). While the scaling of slip with seismic moment of equation (6) is very different from the one dictated by equation (4) for constant stress drop, it is correctly described by a model of interacting multiple asperities embedded in a surrounding zone of weaker coupling (Johnson & Nadeau, 2002), which causes the slip to increment proportionally to $M_0^{1/6}$, and the stress drop to diminish proportionally to $M_0^{-1/4}$ (see Fig. 3). The Parkfield data set and all results are described in details in the Supporting Information, whereas both the methods used to obtain Brune- and ERT-based slip and stress drop estimates are briefly outlined in Appendices.

Based on equations (A1) and (A2) in Appendix A and using the seismic moments with their uncertainties provided by Malagnini and Dreger (2016), the uncertainties of the ERT-based stress drops for the Parkfield repeating earthquakes listed in the catalog by Nadeau and Johnson (1998) are smaller than the dimensions of their symbols in Figure 3, in sharp contrast with the Brune-based stress parameters, which are characterized by large error bars. Estimates of ERT-based stress drop for other repeating earthquakes plotted in Figure 3 do not have uncertainties associated with them.

Corner Frequency vs ERT vs Finite-Source Results

The different scaling with earthquake size inferred for slip estimated by the corner frequency and ERT approaches is very interesting; the slip values retrieved by these two

approaches correlate with different features inferred from the finite-source models: average and peak slip values, respectively. This suggests that corner frequency and ERT approaches are sensitive to different aspects of the rupture history. On one hand, the ERT approach is informing on the peak values, that is, to the high slip concentrations (asperities) characterizing the source model. On the other hand, the corner frequency estimates provide information on the scaling of average slip values.

The observation that the corner frequency methods represent average properties of the rupture history is intuitive, however it is worth examining this through a numerical simulation. Understanding what each method recovers about the source is important to comprehend how heterogeneity in the rupture process can affect source parameters. Calculating ground motion time histories from kinematic rupture models and performing standard spectral analysis can help to shed light on this finding, and to understand the differences between corner-frequency, ERT and FSM slip estimates.

We use a broadband finite-source simulation method based on the multiple time window approach of Hartzell and Heaton (1983) to account for variations in rupture velocity and rise time, and apply a dynamically consistent moment rate spectrum (e.g. Mena et al. 2010). We simulated time histories using an interpolated version of the Wald et al. (1996) slip model for the Northridge earthquake (Figure 4). The model was interpolated to a subfault dimension of 0.10 km, and the rupture velocity and rise time values from Wald et al. (1996) were applied. The slip was distributed into three time windows by assuming a constant slip velocity of 1 m/s. The dynamically consistent slip velocity function (Dreger et al., 2007b; Mena et al., 2010) allows for adjusting the temporal sharpness of the function, and the high-frequency fall-off rate of the spectrum. This is important since to first order the propagating portion of the rupture yields a *1/f* behavior, and the application

of a common triangular slip velocity function and additional $1/f^2$ behavior giving a net greater than $1/f^2$ high-frequency fall-off rate. The function we use yields a net $1/f^2$ high frequency fall-off rate as described below.

From the slip model the stress change is directly computed using the method of Ripperger and Mai (2004) (Figure 4), and the average peak stress drops (and of course slip) can be calculated. Average slip is simply the average of non-zero sub-fault slips. The average stress drop is determined by first considering only non-zero slip sub-faults, and then averaging those that have a stress drop (and not a stress increase). Figure 4 shows the input slip model and the calculated stress change. The peak and average slips in the input model are 297.7 and 70.5 cm, and the peak and average stress drops are 16.3 and 3.9 MPa. The overall rupture area is 302.1 km^2.

In Figure 5 we compare observed and simulated time series and spectra at the Newhall site. Newhall was located in the forward directivity direction and recorded some of the largest ground motions. The finite-source model explains the overall features of the data quite well, and the spectra comparison shows good agreement over the 0.02 to 10 Hz band with a nominal $1/f^2$ high frequency fall off rate.

To estimate the corner frequency for the simulated Northridge event we compute synthetics every 5 degrees in azimuth for stations located at 20 km to fully capture the radiation pattern and rupture directivity effects on the simulated waveforms and spectra. The three-component synthetics were converted to amplitude spectra and summed to average the radiation pattern effects, producing a single composite spectrum for each of the 71 sites.

The spectra were fit with a Brune spectral model with a $1/f^2$ high frequency fall of rate, and an attenuation model that assumes the Q from the velocity model used to compute the Green's

functions used in the simulation. Equation (7) shows the spectral model applied to the synthetic data.

$$\frac{A}{\left(1+\left({}^{f}/_{f_c}\right)^2\right)} e^{\frac{-\pi f r}{Q\beta}} \quad (7)$$

Q and β are assumed from the Wald et al. (1996) velocity model used to compute the Green's functions. The amplitude parameter (A) and corner frequency (f_c) were estimated using a grid search. Sampling the spectrum every 5 degrees averaged the directivity effect on the corner frequency. Of course, in spectral applications to real data, imperfect station coverage could lead to biased estimates of the average corner frequency, and therefore the inferred slip and stress drop parameters. This is something that must be considered in applications to real data. In this case we have optimal coverage and such bias is not an issue.

Figure 6 shows histograms of the fit corner frequency, and estimated Brune slip and stress drop. The distribution reflects the range from forward directivity directions with a maximum value 0.237 Hz to the anti-directivity direction with a minimum of 0.072 Hz. Table 1 lists the average corner frequency assuming both gaussian and log-normal estimates together with the Brune (1970) stress drop and slip.

The fairly large range in corner frequency due to rupture directivity effects and the heterogeneous rupture model leads to large uncertainty in the average Brune slip and area (proportional to corner frequency squared) and the Brune stress drop (proportional to corner frequency cubed). Nevertheless, the average values do compare favorably with the values estimated directly from the finite-source model (Figure 4). For example, the log-normal estimates of corner frequency stress drop and area are 4.7 MPa and 300 km^2, agreeing well with the finite-source estimates of 3.9 MPa and 302 km^2. While there is a difference in the Gaussian and log-normal

estimates of the mean the uncertainties in the parameters are quite large and encompass the values determined directly from the input slip model. This synthetic analysis shows that corner frequency estimates tend to measure the average slip and the average stress drop of an event, however the magnitude of values are dependent upon the choice of the model relating corner frequency to fault parameters. In this case we use Brune (1970) to estimate these parameters however it has been discussed that there is a 5.58 range between estimates based on Brune (1970), Madariaga (1976) and Sato and Hirasawa (1973). The Madariaga (1976) model is the most compact of the three, and rupture area and stress drop values of 95.5 sq. km and 26.6 MPa are found with this model. The rupture area is only 1/3 of the input finite-fault rupture area and the stress drop is more than 5 times larger than the finite-source average, and is in fact larger than the peak stress drop. Albeit only for one finite-fault model we find that the Brune model agrees most closely with estimates of rupture area, slip and stress drop from the Wald et al., (1996) finite-source model.

DISCUSSION

Candela et al. (2011) have presented interesting observations of fault roughness obtained from a global data set of faults of all styles (normal, strike-slip, oblique), as well as for laboratory measurements, suggesting a self-affine slip scaling law similar to that by Nadeau & Johnson (1998). Because fault roughness controls the slip distribution, Candela et al. (2011) suggest that static stress drop during an earthquake is related to the scaling properties of the fault-surface topography. Roughness of natural fault planes, as well as that of laboratory frictional surfaces, is characterized by topographical features whose lateral dimensions and amplitudes are linked by a power law scaling that may be completely described by the average amplitude at a given scale, and the slope of the power law (the Hurst exponent H_R) (Candela et al., 2011). It is found that H_R is less than 1 (H_R~0.6 parallel to the slip direction), implying a deviation from self-similarity.

It may be easily demonstrated (Andrews & Barrall, 2011) that also the scaling of the average stress drop may be written in terms of the same Hurst exponent H_R as: $\Delta\sigma(l) \propto M_0^{(H_R-1)/(H_R+2)}$ (see also Eshelby, 1959). Candela et al. (2011) found that their global data set was consistent with a relationship for stress drop scaling as $M_0^{-0.15}$, which is similar to the Nadeau and Johnson (1998) relationship that stress drop is proportional to $M_0^{-0.25}$.

Mai and Beroza (2002) estimated the Hurst exponent from 42 finite-source models ranging in size from M 5.5 to 8.0 and found an average value of 0.76±0.22 implying a scaling of stress drop with seismic moment ranging from $M_0^{-0.01}$ to $M_0^{-0.18}$. The spread in stress drop scaling is essentially from self-similar to non-self-similar as suggested by Candela et al. (2011) and Nadeau & Johnson (1998). While the exponents are not exactly the same from these different approaches, they significantly have the same sign, arguing that the stress drop decreases as seismic moment increases. Collectively this suggests that scaling is weakly self-affine, or that faults have a higher degree of roughness at lower magnitudes. It is possible that for larger magnitudes, on more mature larger segments of the fault that some of this roughness is eliminated, and evolves to larger length scales.

Our results, shown in Figures 2 and 3, indicate that for earthquakes larger than M 5.5 the Brune-based and ERT-based estimates of seismic slip and stress drop do not show significant differences up to M 7.8. This can be interpreted as a weaker control of small-scale heterogeneities on rupture history for moderate- to large-magnitude earthquakes. This is consistent with the results of both Candela et al. (2011), who find that small scale heterogeneity exists on large exhumed faults, and Mai & Beroza's (2002), who find no moment dependence of the Hurst coefficient in their finite-source database, indicating that finite-source models have a richness in small

wavelength heterogeneity. We do find that the scaling relationship (6) proposed by Nadeau & Johnson (1998) predicts the scaling of peak slip values with seismic moment over a broad moment magnitude range ($-0.7 < M < 7.8$), and that the peak slip values inferred from finite-source models are consistent with this relationship.

We find no evidence for systematic variations of the average Brune-based stress drop for increasing seismic moment, in the magnitude range [0 – 7.8] however the scatter in the estimates is large (Cocco et al., 2016). Malagnini et al. (2014b), as well as other studies (Olsen &Apsel, 1982; Sato & Hirasawa, 1973) have suggested that there may be evidence for intra-sequence (mainshock vs. aftershocks) scaling of stress drop with a sign opposite to what has been found from the ERT-based approach, the geological fault roughness data and from finite-source models. It can be inferred from those studies that the slip power spectrum has a steeper decay than predicted by equation (4), suggesting that aftershock ruptures may have less heterogeneity perhaps due to damage, that could also lead to systematic lowering of corner frequency due to increased attenuation, or more uniform stress distributions due to mainshock loading. This is speculation, as there are not many examples of comparisons between mainshock and aftershock rupture models.

Several observations in the literature (Dreger et al., 2007a; Hartzell & Heaton, 1983; Kim et al., 2016) indicate that repeating earthquakes are also characterized by heterogeneous distributions of slip and stress-drop. We show in this study that ERT-based slip values agree consistently with peak slips from finite-source models. We can interpret this result as an indication that peak slip is associated with the rupture of micro-asperities characterized by a nearly complete stress drop. In Kim et al. (2016) the average slip rate of the most recent three M2.1 Parkfield repeaters, where the repeat times have recovered to pre-2004 rates, is 2.5 cm/yr, nearly the same as the geodetic rate of 2.3 cm/yr. In the study by Kim et al. (2016), the same fault patch with similar overall dimension

was found to rupture repeatedly. The peak slip in the sequential earthquakes is consistent with the Nadeau & Johnson relation, but there is an indication that the patches with peak slip, and possibly the hypocenter, moves from event to event, indicating that the residual stress after the rupture affects the nucleation and the slip distribution in following earthquakes.

In terms of ERT-based estimates of stress drop, the bulk of repeating earthquakes analyzed in this paper, which also provides the most extreme set of values, comes from the transitional segment of the San Andreas fault at Parkfield. It is thus important to verify their behavior in terms of the fault kinematics, and we choose to do so by comparing the cumulative slip during the entire *Epoch 2* time window, at all individual families of repeating earthquakes that had elements in both *Epoch 1* and *Epoch 2*. The comparison is performed between ERT-based and Brune-based estimates of the cumulative slips observed at all individual seismogenic patch where a family of repeaters is located. For the Brune-based estimates of cumulative slip we use an average value for the Brune stress drop of 0.3 MPa (red squares).

ERT-based cumulative slips were calculated using the ERT-based stress drops estimated in Epoch 1 (blue squares in Figure 7), whereas the average Brune stress drops was obtained from the individual results of the 21 events shown in Figure 3. Based on the visual inspection of Figure 7 we state the following: i) all families of repeating earthquakes started at the same background slip rate, which was undisturbed at a background level of 0.023 m/year until the September 28 2004 M6 Parkfield earthquake (light blue vertical line); ii) the post-seismic response to the main shock, modeled as suggested by Perfettini and Avouac (2004), well describes the slip evolution at all locations of the repeaters' families, after the main shock occurred; iii) about two years after the occurrence of the main shock, most of the families were already at the background creep-rate; iv) the fact that the background slip rate is readily reached, and that the post-seismic functional form by Perfettini and

Avouac (2004) is strictly followed by the cumulative slip of all the different families, are clear signs that no significative aseismic creep affects the repeaters. In other words, it is either that the entire slip rate is completely released seismically even after a large disturbance like the 2004 main shock (no partial creep allowed), or, if aseismic slip is allowed on these patches, the percentage of aseismic slip must remain constant at all slip rates (unlikely); v) Brune stress drop-based cumulative slips (red squares) cannot even keep up with the creeping fault's background slip rate; vi) the use of small (repeating) earthquakes as fault creep meters seems justified.

Conclusions

We show differences between the scaling relationships with earthquake size for a complete stress drop ERT model and the Brune corner-frequency model in terms of both slip and stress drop (Figures 2 and 3, respectively). In particular, we show that peak values of slip scale similarly to the complete stress drop ERT model, while average slip and stress values inferred from finite-source models scale consistently with the Brune-based estimates. Peak stress values agree generally with the values inferred for the ERT-based model, although they do not show a clear scaling with seismic moment. Our interpretation of these outcomes relies on the role of heterogeneities of the earthquake source, where the ERT-based estimates are affected by small-scale fault roughness and asperity distribution characterized by a nearly complete stress drop near peak slip regions, while the Brune-based estimates are controlled by the average fault properties. It is of relevance to discuss that while the scaling of peak slip values with seismic moment matches the one inferred by ERT-based slip estimates, peak stress drop does not agree as closely. This can be explained by the larger uncertainties affecting peak stress drop (see Figures S2-S4 in the Supporting Information for an example of finite-source model uncertainty on estimated average and peak stress drops). However, it might be also possible to argue that peak stress drop in areas with slip concentration and peak slip

values does not necessarily correspond to a complete stress drop, but it might range between the complete and the average values of stress drop. It is also interesting to observe that values of peak stress drop do not show a clear trend with earthquake size, similarly to Brune-based estimates and average stress drop values.

The ERT complete stress drop model yields a scaling law in which stress drop decreases as earthquake size increases, in agreement with the self-affine scaling proposed by Candela et al. (2011) as well as with spectral analysis of finite-source slip models (Mai & Beroza, 2002). These results rely on the assumption that the heterogeneities characterizing the earthquake rupture process extend to all resolvable scales. In fact, heterogeneity is observed in laboratory scale frictional sliding models in terms of slip pulse behavior, slip velocity, rupture speed (McClaskey et al., 2015), stress drop and heterogeneity in dimensions of asperities (Passelegue et al., 2016).

The models of Johnson & Nadeau (2002) and Candela et al. (2011) posit that the fault is comprised of asperities of different dimensions and shear strength. Candela et al. (2011) propose a model in which two self-affine surfaces are pressed together. In such a model the short wavelength features will be subjected to higher stress concentrations and the longer wavelength features to lower stress. During rupture the stress drop near the asperities, characterized by small wavelength features, is expected to be larger than the longer wavelength features of the slip distribution, because of the high slip gradient associated with fault roughness. Although finite-source models of large earthquakes seem to be preferentially constrained by the long-wavelength heterogeneity, the associated slip distributions are characterized by Hurst exponents (Mai & Beroza, 2002) similar to those inferred from geologic observations (Candela et al., 2011; Mai & Beroza, 2002). By investigating the source properties of micro-earthquakes using different and complementary approaches we corroborate previous findings concerning the scale dependent properties of faulting

and earthquake ruptures. Despite the inferred heterogeneity at all scales, we do not observe a clear effect on the Brune stress drop scaling with earthquake size. We confirm that the interpretation of the self-similar behavior of stress drop scaling is strongly model dependent.

ACKNOWLEDGMENTS AND DATA

High Resolution Seismic Network data was provided by the Berkeley Seismological Laboratory and NCEDC. All Figures were built using the Generic Mapping Tools v. 4.2.1 (www.soest.hawaii.edu/gmt, Wessel & Smith, 1998). Irene Munafo' was supported by Progetto MISE DGS 2018.

LM analysed most seismic data and drafted the manuscript; IM participated to the data analysis; DD collected most of the data from the finite source models; all authors participated to the discussions on earthquake source physics, and to the editing of the manuscript.

REFERENCES

Aki, A., 1972. Earthquake mechanism, *Tectonophysics,* 13, 423-446.

Andrews, D.J. & Barall, M., 2011. Specifying Initial Stress for Dynamic Heterogeneous Earthquake Source Models, *Bull. Seism. Soc. Am.,* 101, 2408-2417. doi:10.1785/0120110012.

Beresnev, I. A., 2003. Uncertainties in finite-fault slip inversions: To what extent to believe? (A critical review), *Bull. Seismol. Soc. Am*., 93, 2445–2458.

Blanke, A., Kwiatek, G., Goebel, T., Bohnhoff, M., and Dresen, G.H., 2019. Stress Drop, Magnitude and Earthquake Kinematics of Acoustic Emissions observed in Triaxial Stick-Slip Experiments, *AGU Fall Meeting*, San Francisco, CA, 9-13 December 2019, MR23E-0168.

Bletery, Q., Sladen, A., Delouis, B., Vallee, M., Nocquet, J.M., Rolland, L. & Jiang, J., 2014. A detailed source model for the Mw 9.0 Tohoku-Oki earthquake reconciling geodesy, seismology, and tsunami records, *J. Geophys. Res.,* doi:10.1002/2014JB011261.

Brune, J. N., 1970. Tectonic stress and the spectra of seismic shear waves from earthquakes, *J. Geophys. Res.,* 75, 4997-5009.

Brune, J. N., 1971. Correction (to Brune (1970)), *J. Geophys. Res.,* 76, 5002.

Candela, T., Renard, F., Bouchon, M., Schmittbuhl, J. & Brodsky, E., 2011. Stress drop during earthquakes: effect of fault roughness scaling, *Bull. Seism. Soc. Am*., 101, 2369-2387. doi: 10.1785/0120100298.

Cocco, M., Tinti, E., & Cirella, A., 2016. On the scale dependence of earthquake stress drop, *J. Seismol.*, 20:1151–1170. doi 10.1007/s10950-016-9594-4.

Dreger, D.S., Nadeau, R.M., and A. Chung, 2007a. Repeating earthquake finite source models: Strong asperities revealed on the San Andreas Fault, *Geophys. Res. Lett.,* 34, L23302. doi:10.1029/2007GL031353

Dreger, D., E. Tinti, and A. Cirella, 2007b. Slip velocity function parameterization for broadband ground motion simulation, Seismological Society of America 2007 Annual Meeting Waikoloa, Hawaii, 11–13 April 2007.

Eshelby, J.D., 1957. The determination of the elastic field of an ellipsoidal inclusion, and related problems, *Proc. R. Soc. London, Ser. A* 241, 376–396.

Eshelby, J.D., 1959. The elastic field outside an ellipsoidal inclusion, *Proc. R. Soc. London, Ser. A* 252, 561–569. doi:10.1098/rspa.1959.0173.

Hanks, T.C., 1977. Earthquake stress-drops, ambient stress, and the stresses that drive plates, *Pure Appl. Geophys*., 115, 441-458.

Hartzell S.H. & Heaton, T.E., 1983. Inversion of strong ground motion and teleseismic waveform data for the fault rupture history of the 1979 Imperial Valley, California, earthquake, *Bull. Seism. Soc. Am.,* 73, 1553-1583.

Ide, S. & Beroza, G.C., 2001. Does apparent stress vary with earthquake size?, *Geophys. Res. Lett.,* 28, 3349-3352.

Johnson, L.R. & Nadeau, R.M., 2002. Asperity Model of an Earthquake: Static Problem, *Bull. Seism. Soc. Am.,* 92, 672-686. doi: 10.1785/0120000282.

Kanamori, H. & Anderson, D.A., 1975. Theoretical Basis of Some Empirical Relationships in Seismology, *Bull. Seism. Soc. Am*., 65, 1073-1095.

Kaneko, Y. and P. M. Shearer (2014). Seismic source spectra and estimated stress drop derived from cohesive-zone models of circular subshear rupture, Geophys. Journ. Int., 197, 1002-1015, doi:10.1093/gji/ggu030.

Kim, A., Dreger, D.S., Taira, T. & Nadeau, R.M., 2016. Changes in repeating earthquake slip behavior following the 2004 Parkfield main shock from waveform empirical Green's functions finite-source inversion, *J. Geophys. Res.,* 121, 1910-1926. doi:10.1002/2015JB012562.

Madariaga, R., 1976. Dynamics of an expanding circular fault, *Bull. Seism. Soc. Am.,* 66, 639-666.

Mai, P.M. & Beroza, G.C., 2002. A spatial random field model to characterize complexity in earthquake slip, *J. Geophys. Res.,* 107, 2308. doi: 10.1029/2001JB000588.

Mai, P. M., Schorlemmer, D., Page, M., Ampuero, J-P., Asano, K., Causse, M., Custodio, S., Fan, W., Festa, G., Galis, M., Gallovic, F., Imperatori, W., Kaser, M., Malytskyy, D., Okuwaki, R., Pollitz, F., Passone, L., Razafindrakoko, H. N. T., Sekiguchi, H., Song, S. G., Somala, S. N., Thingbaijam, K. S., Twardzik, C., van Driel, M., Vyas, J. C., Wang, R., Yagi, Y., and Zielke, O., 2016. The Earthquake-Source Inversion Validation (SIV) Project, *Seism. Res. Lett.*, 87(3), doi: 10.1785/0220150231.

Malagnini, L. & Dreger, D.S., 2016. Generalized Free Surface Effect and Random Vibration Theory: A New Tool for Computing Moment Magnitudes of Small Earthquakes using Borehole Data, *Geophys. J. Int.,* 206, 103-113.

Malagnini, L., Munafo', I., Cocco, M., Nielsen, S., Mayeda, K. & Boschi, E., 2014a. Gradual fault weakening with seismic slip: inferences from the seismic sequences of L'Aquila,

2009 and Northridge, 1994, *Pure and Applied Geophysics.,* doi:10.1007/s00024-013-0752-0.

Malagnini, L., Mayeda, K., Nielsen, S., Yoo, S.H., Munafo', I., Rawles, C. & Boschi, E., 2014b. Scaling transition in earthquake sources: a possible link between seismic and laboratory measurements, *Pure and Applied Geophysics*., doi:10.1007/s00024-013-0749-8.

Malagnini, L., S. Nielsen, K. Mayeda, and E. Boschi (2010), Energy radiation from intermediate- to large-magnitude earthquakes: Implications for dynamic fault weakening, J. Geophys. Res., 115, B06319, doi:10.1029/2009JB006786.

Mayeda, K. & Malagnini, L., 2009. Apparent stress and corner frequency variations in the 1999 Taiwan (Chi-Chi) sequence: Evidence for a step-wise increase at Mw ~ 5.5, *Geophys. Res. Lett*., 36, L10308. doi:10.1029/2009GL037421.

Mayeda, K., Malagnini L., and Walter, W. R., (2007). A new spectral ratio method using narrow band coda envelopes: Evidence for non-self-similarity in the Hector Mine sequence, Geophys. Res. Lett., 34, L11303, doi:10.1029/2007GL030041.

McLaskey, G. C., Kilgore, B. D., and Beeler, N. M., 2015. Slip-pulse rupture behavior on a 2 m granite fault, Geophys. Res. Lett., 42, 7039–7045, doi:10.1002/2015GL065207.

Mena, B., Mai, P. M., Olsen, K. B., Purvance, M. D., and Brune, J., 2010. Hybrid broadband ground-motion simulatin using scattering Green's functions: Application to large-magnitude events, *Bull. Seism. Soc. Am*., 100, 5A, 2143-2162.

Nadeau, R. M. & Johnson, L.R., 1998. Seismological studies at Parkfield VI: Moment release rates and estimates of source parameters for small repeating earthquakes, *Bull. Seismol. Soc. Am.,* 88, 790–814.

Noda, H., Lapusta, N. & Kanamori, H., 2013. Comparison of average stress drop measures for ruptures with heterogeneous stress change and implications for earthquake physics, *Geophys. J. Int.,* 193, 1691-1712.

Olsen, A. H. & Apsel, R.J., 1982. Finite faults and inverse theory with application to the 1979 Imperial Valley earthquake, *Bull. Seism. Soc. Am*., 72, 1969-2001.

Passelègue, F. X., A. Schubnel, S. Nielsen, H. S. Bhat, D. Deldicque, and R. Madariaga (2016), Dynamic rupture processes inferred from laboratory microearthquakes, *J. Geophys. Res.* Solid Earth, 121, 4343–4365, doi:10.1002/2015JB012694.

Perfettini, H., and Avouac, J.-P., 2004. Postseismic relaxation driven by brittle creep: A possible mechanism to reconcile geodetic measurements and the decay rate of aftershocks, application to the Chi-Chi earthquake, Taiwan, *J. Geophys. Res*., 109, B02304, doi:10.1029/2003JB002488.

Ripperger, J. & Mai, P.M., 2004. Fast computation of static stress changes on 2D faults from final slip distribution, *Geophys. Res. Lett.,* 31, L18610. doi: 10.1029/2004GL020594.

Sato, T. & Hirasawa, T., 1973. Body Wave Spectra from the Propagation Shear Cracks, *J. Phys. Earth.,* 21, 415-431.

Schmidt, D.A., Burgmann, R., Nadeau, R. M. & d'Alessio, M., 2005. Distribution of aseismic slip rate on the Hayward fault inferred from seismic and geodetic data, *J. Geophys. Res*., 110, B08406. doi:10.1029/2004JB003397.

Taira, T., Dreger, D. S. & Nadeau, R.M., 2015. Rupture process for micro‐earthquakes inferred from borehole seismic recordings, *Int. J. Earth Sci., (Geol Rundsch)* 104, 1499–1510. doi:10.1007/s00531-015-1217-8.

Titus, S.J., DeMets, C. & Tikoff, B., 2005. New slip rate estimates for the creeping segment of the San Andreas fault, *Geology* 33, 205–208.

Titus, S.J., DeMets, C. & Tikoff, B., 2006. Thirty-five-year creep rates for the creeping segment of the San Andreas fault and the effects of the 2004 Parkfield earthquake: Constraints from alignment arrays, continuous Global Positioning System, and creepmeters, *Bull. Seismol. Soc. Am*., 96, S250–S268. doi:10.1785/0120050811.

Wald, D.J., Heaton, T.H., and Hudnut K.W., 1996. The slip history of the 1994 Northridge, California, earthquake determined from strong-motion, teleseismic, GPS, and leveling data, *Bull. Seism. Soc. Am.,* 86, pp. S49-S70.

Wang, K., Dreger, D. S., Tinti, E., Burgmann, R., and Taira, T., 2020. Rupture process of the 2019 Ridgecrest, California M6.5 Foreshock and M7.1 Earthquake Constrainted by Seismic and Geodetic Data, in review *Bull. Seism. Soc. Am*.

Wessel, P. & Smith, H.F., 1998. New, improved version of generic mapping tools released, *Earth Space Sci. News,* 79. doi: 10.1029/98EO00426.

Zollo, A., Orefice, A. & Convertito, V., 2014, Source parameter scaling and radiation efficiency of microearthquakes along the Irpinia fault zone in southern Apennines, Italy, *J. Geophys. Res. Solid Earth,* 119, 3256–3275. doi:10.1002/2013JB010116.

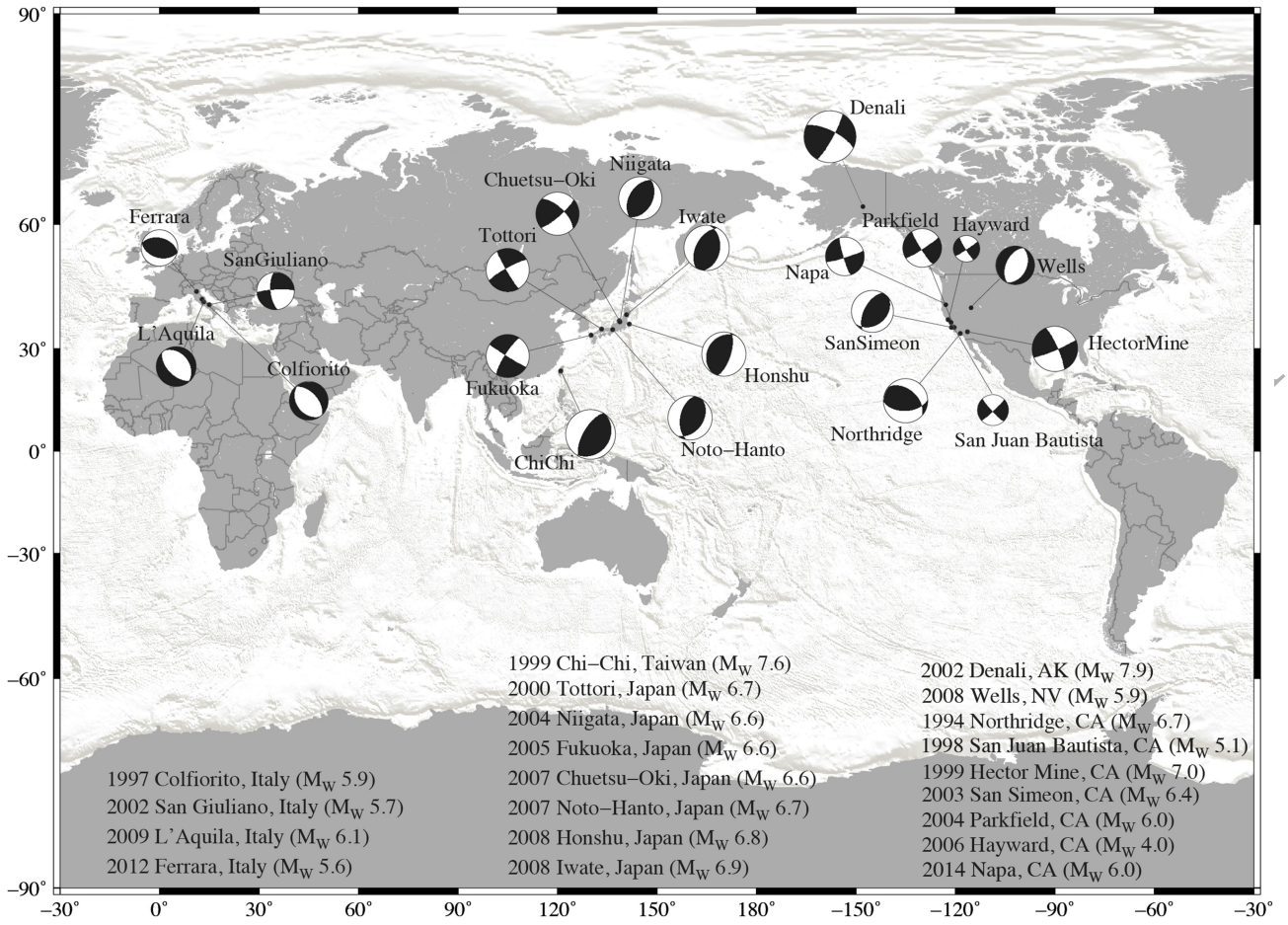

Figure 1. Locations and main shock focal mechanisms of the 21 seismic sequences analyzed in this study. A description of the investigated data set is given in the main text, and further information are available in the papers by Malagnini et al. (2014a,b).

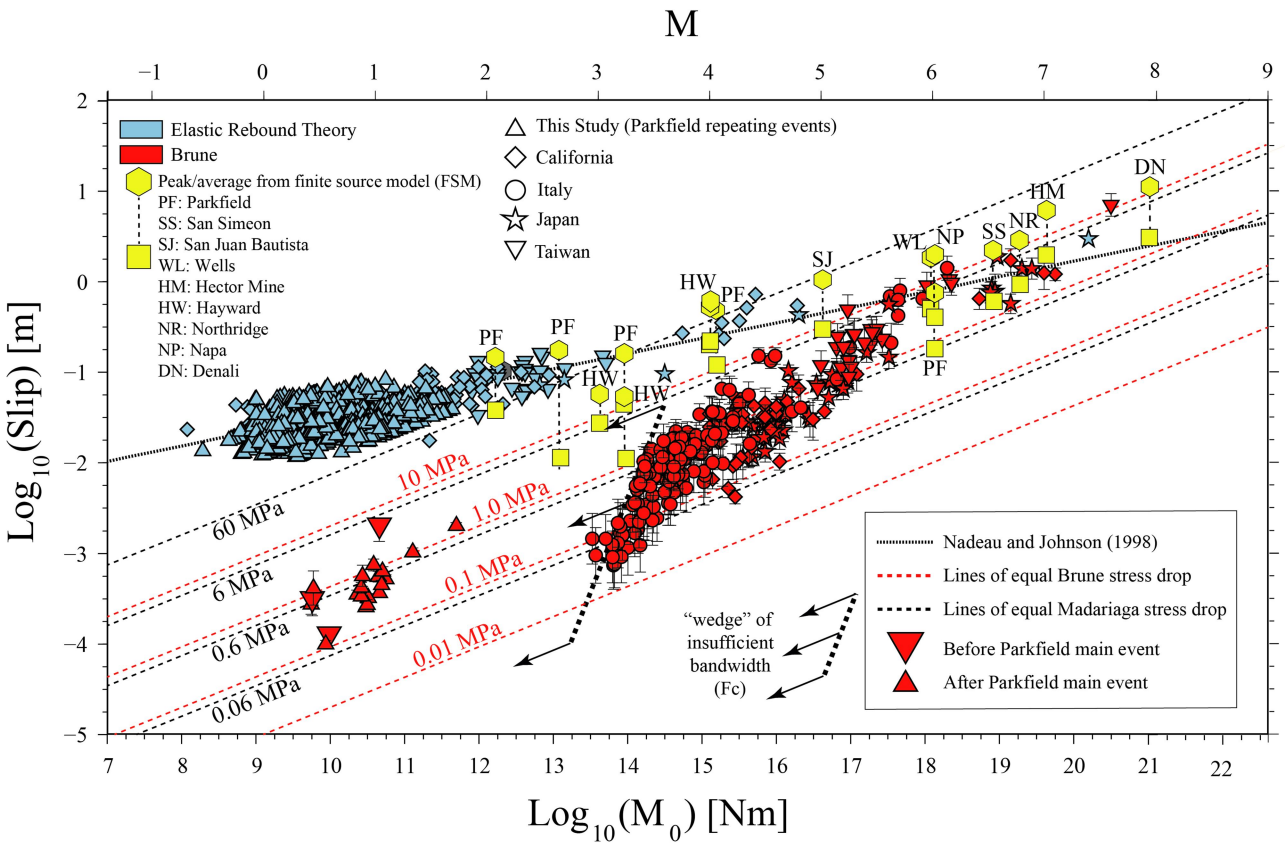

Figure 2. Seismic slip as a function of seismic moment. Red symbols: estimates of slip based on the Brune spectral model calculated by Malagnini et al. (2014a), with the exception of the triangles (which refer to the present study) and slip values from the L'Aquila seismic sequence, which were calculated by Malagnini et al. (2014a); cyan symbols: estimates of ERT-based seismic slip; yellow symbols: peak and average slip values (yellow squares and hexagons, respectively) estimated from kinematic finite fault models. The indicated "wedge" of insufficient bandwidth is due to insufficient S/N ratios in the high-frequency part of the spectra (surface Italian stations); sampling-rate-related issues would start kicking in at the same surface stations, operated at 100 sps, at about **M** 2.5.

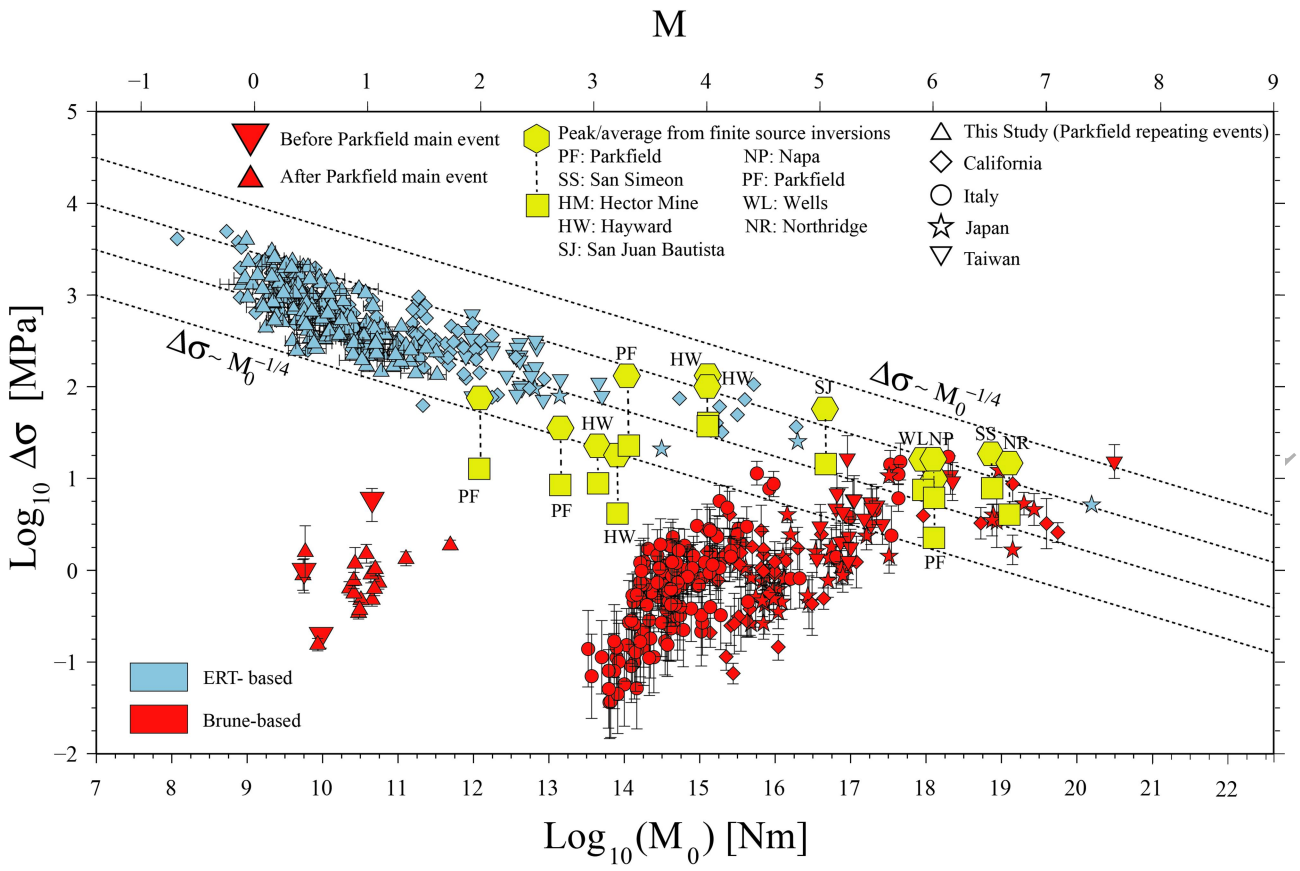

Figure 3. Stress drop as a function of seismic moment. Cyan symbols: ERT-based stress drops obtained in this study for the earthquakes mapped in Figure S1 in the Supporting Information. Triangles are the Brune stress drop values obtained in this study for the Parkfield's clusters of repeating earthquakes. Diamonds represent the results of several studies in California, including that by Nadeau & Johnson (1998). Other symbols indicate earthquakes from other specific regions of the world. Red symbols: Brune-like stress drops. Triangles represent stress drops of 21 Parkfied repeating events; other red symbols are relative to several other seismic sequences analyzed by Malagnini et al. (2014a). Yellow symbols: hexagons represent FSM-based peak stress drops; squares represent average FSM-based stress drops of the same earthquakes. Dotted lines: theoretical stress drop scaling for ERT-based parameters ($\Delta\tau \propto M_0^{-1/4}$), as proposed by Johnson & Nadeau (2002). Lines were arbitrarily pinned to $\Delta\sigma = 10$ MPa, 3 MPa, 1 MPa, and 0.3 MPa at M8.

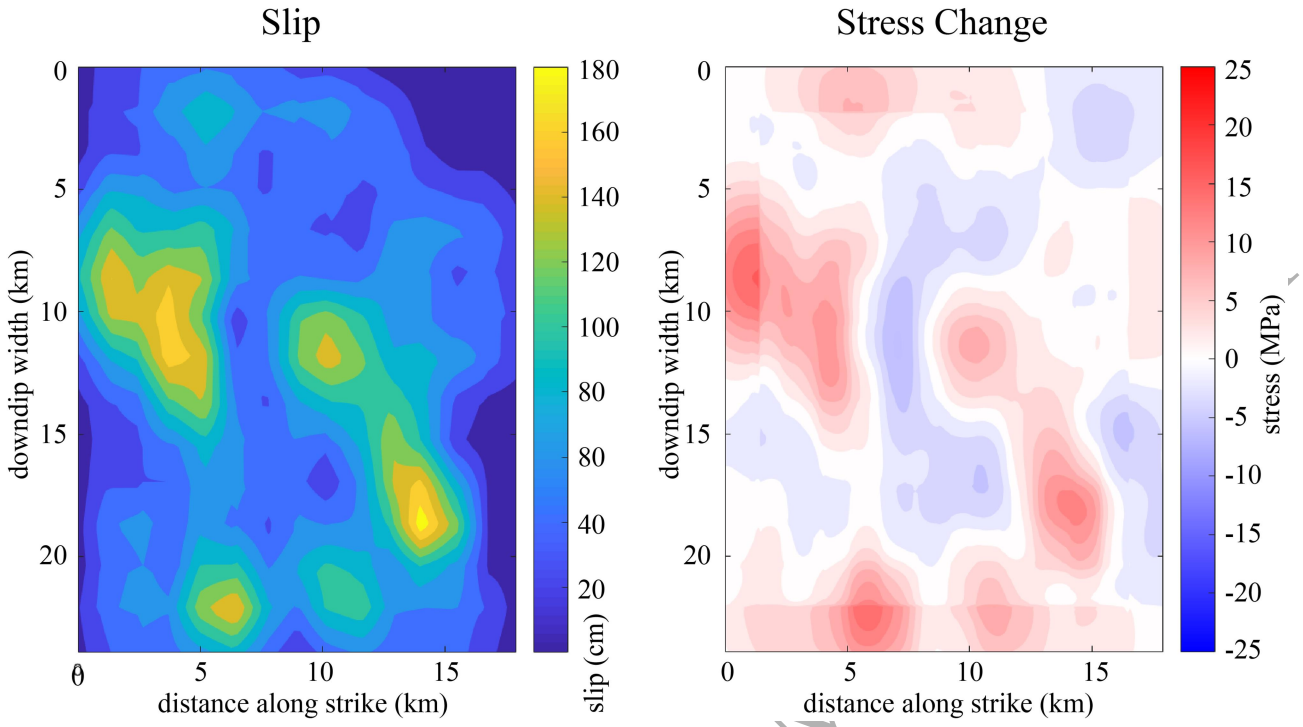

Figure 4. Left: The input strong-motion slip model from Wald et al. (1996). **Right:** The stress change from Ripperger and Mai (2004). Red colors indicate stress drop.

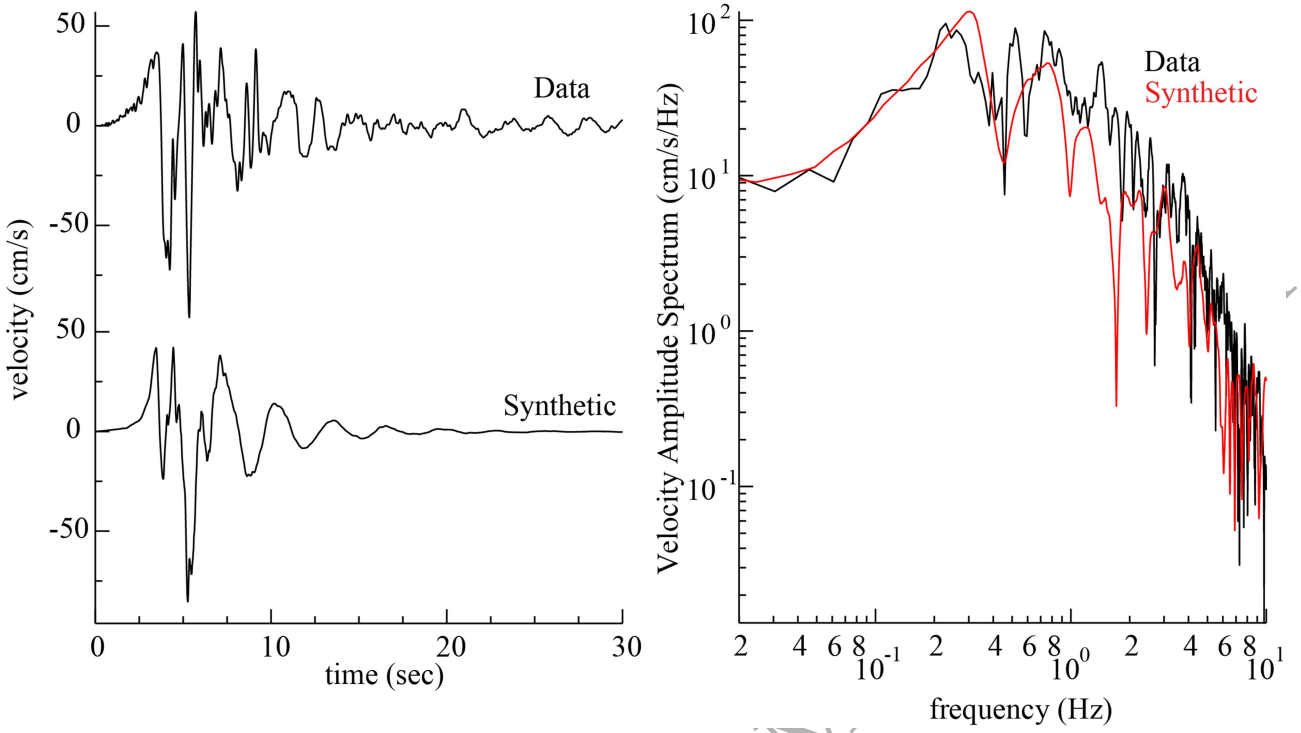

Figure 5. Left: The observed and synthetic velocity seismograms at the Newhall stations. The synthetic was computed with the slip model in Figure 4. **Right:** The observed (black) and synthetic (red) velocity amplitude spectrum. The agreement is good over the 0.02 to 10 Hz passband.

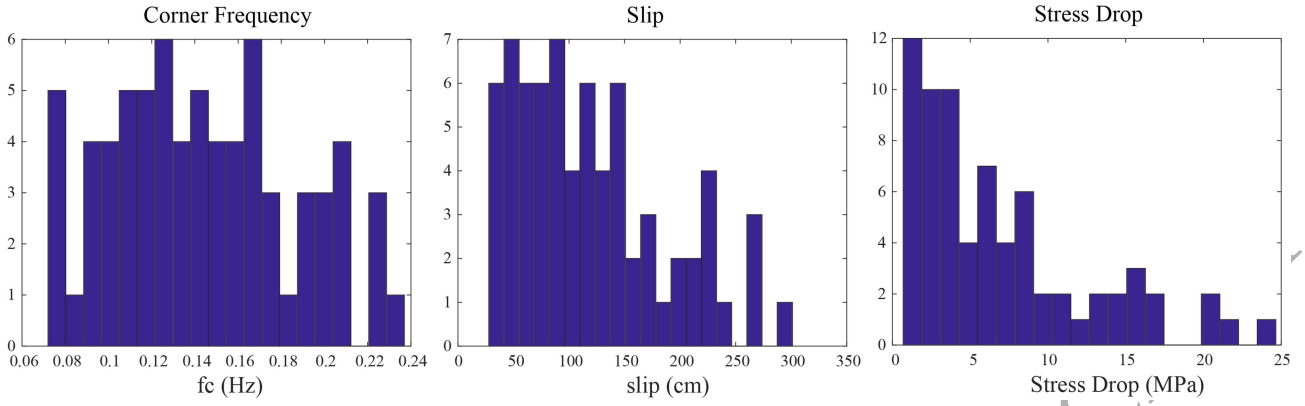

Figure 6. Left: Corner frequency from fitting the Brune model to synthetic spectra. **Middle:** Brune average slip, and **Right:** Brune stress drop. Table 1 lists the average and standard deviation assuming both a gaussian and long-normal distribution.

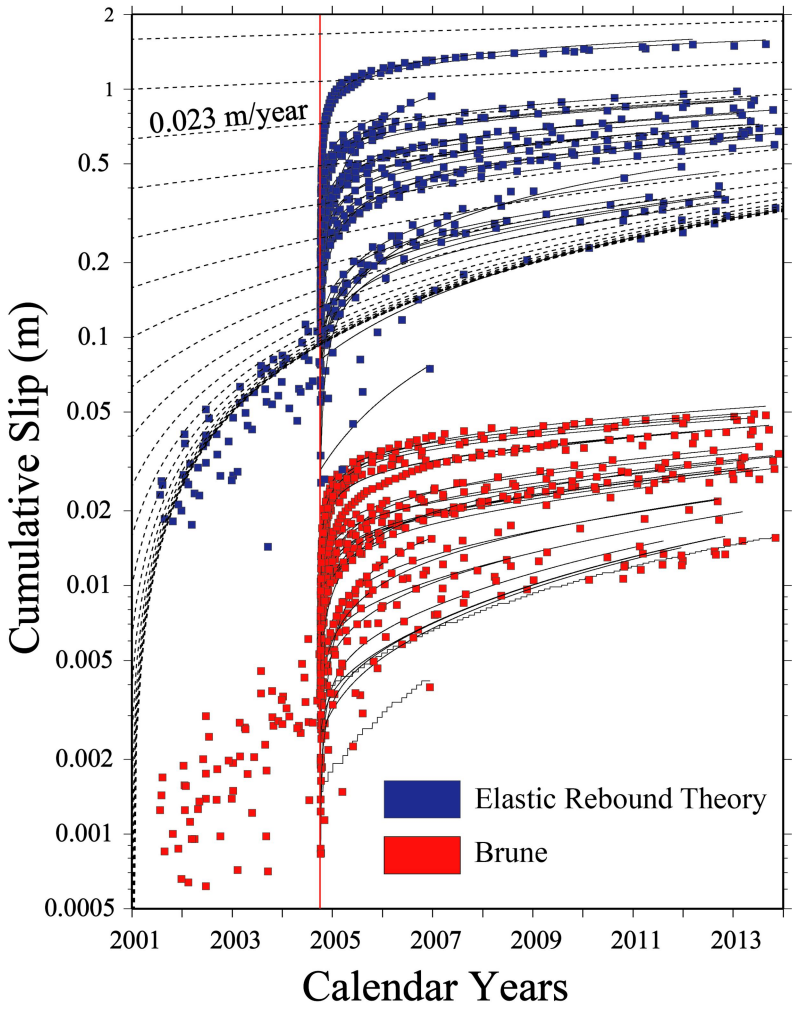

Figure 7. Based on the ERT-based stress drops plotted in Figure 3, which were estimated on earthquakes from Epoch 1, the cumulative slip was computed in Epoch 2 for each family that had events in both Epoch 1 and Epoch 2 (blue symbols). At the occurrence of the M6 2004 Parkfield earthquake, for each family's cumulative slip history we calculated a best-fit curve using the functional form by Perfettini and Avouac (2004) (solid lines). The dashed lines describe a constant 0.023 m/year creep, that is asymptotically reached by the cumulative slips of most families within a couple of years since the occurrence of the main shock. In red are the slip estimates for the same families of repeaters, calculated using a Brune stress drop of 0.3 MPa.

Table 1: Corner frequency estimates of Slip and Stress Drop

	fc + σ (Hz)	Slip + σ (cm)	Stress Drop + σ (MPa)	Area + s (sq. km)
Gaussian	0.143 +- 0.043	112.0 +- 68.7	6.9 +- 5.8	365.6 +- 251.2
Log-normal	0.137 +- 0.036	100.8 +- 46.5	4.8 +- 2.9	300.3 +- 138.7

APPENDICES

A. ERT-based slips and stress drops

We calculate the stress drop needed to match the plate velocity at each cluster (v_{plate} = 0.023 m/year[12ß]), in the undisturbed time window between 1987 and June 1998. The following equation is used to estimate the stress drops plotted in Figure 3 (Candela et al., 2011; Eshelby, 1957; Eshelby, 1959; Mai & Beroza, 2002). Subscript *i* refers to the *i-th* earthquake, and T_j is the time length of "undisturbed" activity for the *j-th* cluster (no post-seismic response acts during T_j):

$$\langle \Delta\tau \rangle_j = \left(\frac{7}{16}\right)\left(\frac{\mu\pi T_j v_{plate}}{\sum_{i=1}^{N_j} M_{0ij}^{1/3}}\right)^{3/2} . \quad \text{(A1)}$$

We calculate the slip values plotted in Figure 2 (cyan triangles) knowing the seismic moment of the *i-th* earthquake and the stress drop of the *j-th* cluster to which the quake belongs:

$$S_{ij} = \frac{M_{0ij}^{1/3}}{\mu\pi}\left(\frac{16\langle \Delta\tau \rangle_j}{7}\right)^{2/3} . \quad \text{(A2)}$$

B. Brune stress drops from fitting source spectral ratios

Source spectral ratios between the mainshock and all the aftershocks can easily be calculated from the source terms computed by Malagnini & Dreger (2016). Theoretical ratios between the moment-rate spectra of two generic events, #1 and #2, can be written as follows:

$$\frac{\dot{M}_1(f)}{\dot{M}_2(f)} = \frac{M_{0_1}\left(1+\left(\frac{f}{f_{c_2}}\right)^2\right)}{M_{0_2}\left(1+\left(\frac{f}{f_{c_1}}\right)^2\right)}, \tag{B1}$$

where M_{0i} is the seismic moment of the *i-th* event [i=1,2]. Two asymptotes characterize eq. (B1): $\frac{M_{0_1}}{M_{0_2}}$ at low-frequency, and, if self-similarity holds, $\left(\frac{M_{0_1}}{M_{0_2}}\right)^{1/3}$ at high frequency (Mayeda & Malagnini, 2009). From the corner frequencies we obtain the Brune stress drops and slips.